International Journal of Heat and Mass Transfer 52 (2009) 3805–3817

Contents lists available at ScienceDirect

International Journal of Heat and Mass Transfer

journal homepage: www.elsevier.com/locate/ijhmt

Effects of carbon nanotube coating on flow boiling in a micro-channel

Vikash Khanikar, Issam Mudawar *, Timothy Fisher

Boiling and Two-Phase Flow Laboratory (BTPFL) and Birck Nanotechnology Center, School of Mechanical Engineering, Purdue University, West Lafayette, IN 47907-2088, USA

ARTICLE INFO

Article history:
Received 2 October 2008
Received in revised form 9 February 2009
Accepted 9 February 2009
Available online 4 May 2009

Keywords:
Flow boiling
Micro-channel
Carbon nanotubes

ABSTRACT

Experiments were performed to assess the heat transfer enhancement benefits of coating the bottom wall of a shallow rectangular micro-channel with carbon nanotubes (CNTs). Using water as working fluid, tests were performed with a bare copper surface and three separate, yet identical CNT-coated surfaces. Each of the CNT-coated surfaces was tested repeatedly at the same mass velocity to explore any time dependence of heat transfer performance parameters, especially critical heat flux (CHF). Appreciable differences in the influence of CNT coating were observed at high mass velocities as compared to low. CHF was repeatable at low mass velocities but degraded following repeated tests at high mass velocities, proving high flow velocities cause appreciable changes to the morphology of the CNT-coated surface. SEM images show the initially near-vertical CNTs were bent upon the heated surface at high mass velocities to form a repeated '*fish-scale*' pattern. Voids between the '*fish scales*' provided near-zero-angle cavities that enhanced heat transfer in the nucleate boiling region compared to the bare copper surface. While CHF was enhanced by the increased heat transfer area associated with the CNT coating, the enhancement decreased following repeated tests as the CNT fin effect was compromised by the bending.

1. Introduction

Over the past 50 yrs, enhancing signal speed and functionality of electronic devices have been realized mostly by miniaturizing electronic components and packaging an increasing number of components in the device itself. Accompanying this trend has been a steady rise in the amount of heat that is dissipated from the device. While this problem was initially handled quite effectively with air cooling schemes, heat dissipation increased to levels that necessitated the use of liquid-cooling schemes that capitalize upon the superior thermophysical properties of liquid coolants compared to air. Yet even these liquid-cooling schemes have recently fallen short of removing the heat for certain advanced devices while maintaining acceptable device temperatures. This explains the emphasis many researchers are presently placing on the implementation of phase-change cooling schemes, especially those involving high coolant velocities, such as micro-channel, jet and spray [1].

One of the simplest forms of convective two-phase cooling is to supply a dielectric coolant parallel to the device's surface. Mudawar and Maddox [2] explored subcooled flow boiling of FC-72 on a simulated electronic device in a vertical rectangular channel. Increasing the coolant's velocity enhanced the single-phase heat transfer coefficient, delayed of onset of boiling to higher heat fluxes and increased critical heat flux (CHF). CHF was associated with bubble coalescence into fairly continuous vapor blankets that inhibited liquid access to the heated surface. However, the shape and size of the vapor blanket was highly dependent on velocity. For low velocities, a continuous vapor blanket encased the entire heated surface and CHF resulted from dryout of a liquid sublayer beneath the blanket. At high velocities, CHF was triggered by dryout beneath smaller discrete vapor blankets. Increasing liquid subcooling was especially effective at enhancing CHF. Aside from its ability to absorb a significant fraction of the supplied energy in the form of sensible heat prior to vaporization, highly subcooled flow greatly decreased bubble size, bringing the bulk liquid in close proximity to the heated surface. Channel size also has a measurable influence on flow boiling performance and CHF. In a study on the effects of channel height, Willingham and Mudawar [3] showed decreasing channel height causes a substantial increase in void fraction, causing CHF to occur as a result of downstream dryout.

Two-phase micro-channel cooling is an extreme form of convective flow boiling where hydraulic diameter is reduced to the range of 100–1000 μm [1]. The merits of a very small hydraulic diameter are readily apparent for laminar single-phase flow, where a constant Nusselt number implies the single-phase heat transfer coefficient is inversely proportional to hydraulic diameter. For two-phase flow, the merits of micro-channel flow are closely associated with fast fluid acceleration along the micro-channel and close proximity of the bulk liquid to the heated surface. Qu and Mudawar [4–6] showed that two-phase micro-channel flow greatly enhances the heat transfer coefficient and helps maintain

* Corresponding author. Tel.: +1 765 494 5705; fax: +1 765 494 0539.
E-mail address: mudawar@ecn.purdue.edu (I. Mudawar).

0017-9310/$ - see front matter © 2009 Elsevier Ltd. All rights reserved.
doi:10.1016/j.ijheatmasstransfer.2009.02.007

Nomenclature

A_t	bottom wall area of micro-channel (also top surface area of copper block)
CHF	critical heat flux
CNT	carbon nanotube
D_h	hydraulic diameter
G	mass velocity
H_{ch}	height of micro-channel
H_{th}	distance between thermocouple and bottom wall of micro-channel
k_s	thermal conductivity of copper block
L	length of micro-channel
P	pressure
q''	heat flux from bottom wall of micro-channel (based on A_t)
q''_m	critical heat flux from bottom wall of micro-channel (based on A_t)
Re	Reynolds number
T	temperature
T_{tci}	temperature measured by thermocouple *tci* (i = 1–4)
$T_{w,tci}$	surface temperature at z_{tci} (i = 1–4)
W_{ch}	width of micro-channel
z	stream-wise location

Subscripts

ch	micro-channel
in	module inlet
out	module outlet
s	solid
tci	thermocouple i (i = 1–4)
w	bottom wall of micro-channel.

better surface temperature uniformity than with single-phase micro-channel flow. However, these advantages are sometimes realized at the expense of increased pressure drop, which places stringent lower limits on micro-channel size. This explains the need for new innovative surface enhancement schemes that would help achieve the cooling merits of two-phase micro-channel flow while avoiding the extremely small sizes responsible for excessive pressure drop. This is a key objective of the present study.

1.1. Heat transfer enhancement with carbon nanotubes

Ever since their discovery, researchers have studied CNTs for different engineering applications their unique electrical, thermal and mechanical properties. CNTs take the shape of extremely thin tubes of graphitic carbon with typical outer diameters ranging from 1 to 100 nm and lengths from 1 to 50 μm. They exist in single-walled (SWCNT) or multi-walled (MWCNT) forms. SWCNTs are made from a single graphene sheet with hexagonally arranged groups of carbon atoms whereas MWCNTs have multiple co-axial graphene sheets. Kim et al. [7] showed that MWCNTs possess thermal conductivities in excess of 3000 W/m K at room temperature, and such observations explain the recent strong interest in implementing CNTs for thermal applications.

Ujereh et al. [8] explored the enhancement potential of CNTs in pool boiling of FC-72 on silicon and copper surfaces. Compared to bare substrates, CNT-coated surfaces reduced the incipient boiling superheat and enhanced the nucleate boiling heat transfer coefficient. These advantages were attributed to the effectiveness of CNTs at both initiating and sustaining the nucleation process; better nucleate boiling heat transfer was also believed to result from increased surface area. An abundance of nucleation sites was observed on the CNT-coated surface because of effective vapor embryo entrapment. The vapor entrapment is of paramount importance to initiating and sustaining the nucleation process in low contact angle coolants such as FC-72, where liquid can easily penetrate and flood cavities, depriving these cavities from viable vapor embryos. With CNTs, vapor entrapment is improved with the creation of near-zero-angle cavities from parallel vertical CNTs and CNT mesh formations that provide an ideal environment for bubble nucleation. Ujereh et al. observed significant CHF enhancement with CNT coatings for both silicon and copper substrates because of increased surface area. Launay et al. [9] showed that, at very low superheats, pool boiling heat transfer with PF-5060 was enhanced using a CNT coating when compared with bare silicon. However, CNTs degraded performance close to CHF. They attributed the differences in enhancement at different heat fluxes to contact resistance between the CNTs and the surface. In addition to contact resistance effects, differences in nucleate boiling performance between the studies of Ujereh et al. and Launay et al. can be attributed to differences in the CNT growth process and anchoring to the surface; both also have a strong bearing on contact resistance. Dujardin et al. [10] showed that CNTs increase nucleation site density in water and most low surface tension fluids.

Most recently, Chakrapani et al. [11] demonstrated the formation of cellular CNT patterns following fluid evaporation from a CNT-coated horizontal surface. Near-vertical CNTs were bunched together to form raised outer walls for the cells, while the cell centers consisted of CNTs that were bent and folded completely upon the surface. Chakrapani et al. attributed this cellular formation to capillary forces that are exerted on the nanotubes during evaporation and strong van der Waals forces between nanotubes. In fact, CNTs possess a high degree of flexibility in bending [12] and can therefore easily deform in response to external forces.

In flow boiling situations, two effects are expected to influence CNT coatings: bubble formation and bulk flow. Given the vigor of the boiling process, it is conceivable that CNTs would deform as bubbles are formed and depart from a CNT-coated surface. Stresses exerted by the bulk flow could induce profound directional morphological changes to the CNT coating.

Recently, the authors of the present study explored flow boiling and CHF trends for a single 10.0-mm wide by 0.371-mm high micro-channel whose bottom copper surface was coated with CNTs [13]. Using water as working fluid, the CNT-coated surface initiated boiling at a lower heat flux and with greater abundance and intensity than a bare copper surface. However, CHF enhancement trends were somewhat erratic, and depended on both mass velocity and inlet subcooling. They postulated that CNT arrays enhance CHF by increasing heat transfer area as well as by serving as very high conductivity fins that penetrate into the cooler, bulk liquid to take advantage of the bulk subcooling away from the wall. Their results suggest high flow velocities tend to fold CNT arrays upon the wall, compromising the fin effect. The hypothesis of substantial fin enhancement requires further investigation, as the convective environment, CNT geometry, and CNT thermal conductivity suggest that fin effects could be significant for a length of order 10 μm from the base; however, radial solid–fluid boundary resistance [14], interfacial base resistance [15], and reduced thermal conductivity due to defects would act to moderate the fin effect.

Recently, the authors conducted additional micro-channel flow boiling tests which indicated that reproducing CHF results by

repeating tests under certain flow conditions is quite elusive. The new findings proved changes to the morphology of the CNT-coated surface are time-dependent. Furthermore, the percentage change in CHF magnitude was very different for high mass velocities as compared to low. These anomalies are the key motivation for the present study.

In the present study, a new systematic operating procedure is used, where three different but identically prepared CNT-coated surfaces are fabricated, one for each of three mass velocity series of tests. Each surface is tested repeatedly at the same mass velocity and inlet subcooling to identify any time-dependent changes in such key flow boiling parameters as single-phase convective heat transfer coefficient, onset of boiling, two-phase flow pattern, nucleate boiling heat transfer coefficient, and CHF. Results are also compared to those of a bare copper surface to assess the overall enhancement potential of the CNT coating.

2. Experimental methods

2.1. Test module

Fig. 1(a) depicts the construction of the test module used in this study. The main components of the test module are an oxygen-free copper block, a thermally-insulating G-7 fiberglass plastic housing, a polyetherimide thermoplastic (GE Ultem 1000) cover plate and twelve cartridge heaters. The copper block is inserted upwards through the central cavity of the G-7 housing and, as shown in Fig. 1(b), a single 10.0-mm wide by 0.371-mm high micro-channel is formed when the cover plate is clamped atop. Inlet and outlet plenums are formed in the housing to ensure uniform flow distribution. Each plenum contains deep and shallow cavities. A small protruding platform around the periphery of the copper block ensures that the bottom wall of the micro-channel is flush with the base of the shallow cavity in each plenum. The top $44.8 \times 10.0\ mm^2$ surface of the copper block constitutes the heated bottom surface for the micro-channel. The twelve cartridge heaters are inserted in bores in the underside of the copper block to supply heat to the surface. The heaters are powered by a 0–110 VAC variac and their total electrical power input is measured by a wattmeter. Four type-K thermocouples are inserted in the copper block a short distance below the micro-channel's heated surface. They are designated *tc1* to *tc4* starting with the one closest to the micro-channel inlet. A ceramic plate is pressed against the underside of the copper block, providing thermal insulation as well as support for the cartridge heaters. A thick G-10 fiberglass plastic plate is placed beneath the ceramic plate to provide both structural support and added insulation. Table 1 provides key dimensions of the micro-channel and the copper block.

Table 1
Key dimensions of micro-channel and copper block.

W_{ch} [mm]	H_{ch} [mm]	L [mm]	H_{th} [mm]
10	0.371	44.8	1.24

2.2. Flow loop

Fig. 2 shows a schematic of the flow loop that delivers deionized water to the test module at the desired flow rate, pressure and temperature. A gear pump supplies the water from the loop's reservoir into a filter, followed by one of two parallel rotameters, and two plate-type heat exchangers before entering the test module. Water from a constant temperature bath is circulated through the two heat exchangers to control the test module's inlet temperature. Control valves situated both upstream and downstream of the test module are used to set the desired test module's outlet pressure as well as to minimize flow or pressure oscillations in the test module. A third heat exchanger is situated downstream of the test module to remove the heat supplied by the test module and the pump. Table 2 provides the operating conditions for the study.

2.3. Operating procedure

A systematic and consistent operating procedure is adopted throughout the study. Prior to conducting a test, the deionized

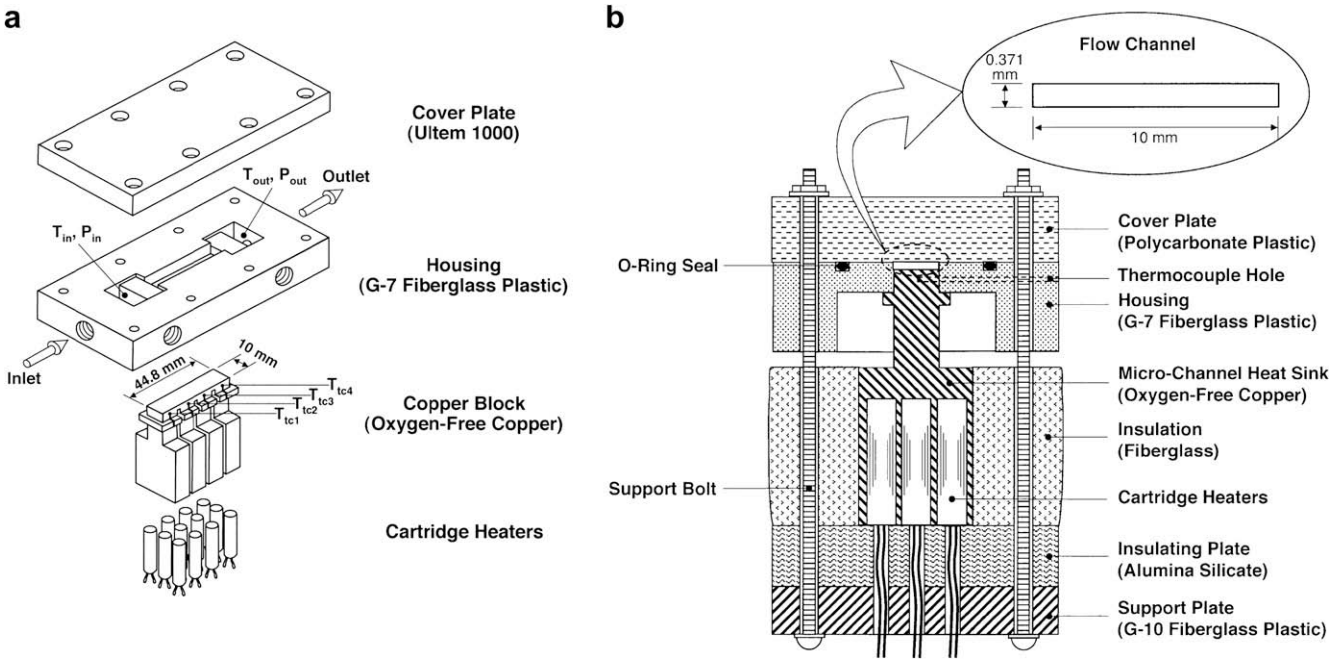

Fig. 1. (a) Main components and (b) sectional assembly view of test module.

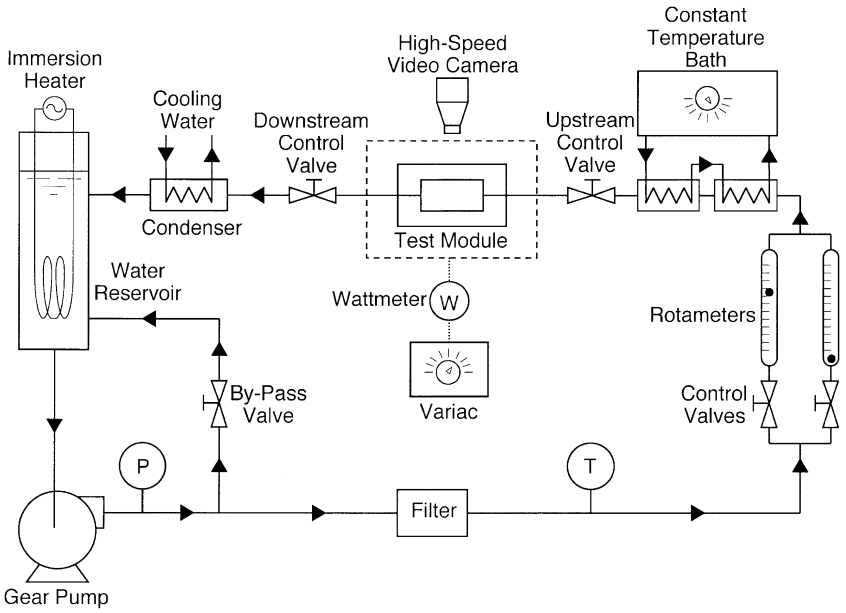

Fig. 2. Schematic of two-phase flow loop.

Table 2
Operating conditions for present study.

Coolant	T_{in} [°C]	G [kg/m^2 s]	Re	P_{out} [bar]
Deionized water	30	86, 228, 368	76–327	1.13
	60	86, 228, 368	131–562	1.13

water is vigorously boiled inside the loop's reservoir to purge any dissolved gases into the ambient. Subsequently, the flow rate, module inlet temperature and outlet pressure are set to yield the desired operating conditions for the test. Electrical power is then supplied to the copper block's cartridge heaters in a small increment. Once the temperatures in the copper block reach steady state, the inlet and outlet pressures (P_{in} and P_{out}), the inlet and outlet temperatures (T_{in} and T_{out}), and the copper block's thermocouple temperatures (T_{tc1} to T_{tc4}) are all recorded using an HP data acquisition system interfaced to a PC. Heat flux, q'', from the heated surface is defined as the measured electrical power input divided by the heated surface area of $A_t = 44.8 \times 10.0$ mm^2. Once all measurements are made, the electrical power is increased again and measurement procedure repeated. The test is terminated when CHF is encountered, which is detected by an unsteady rise in the copper block's temperature.

2.4. Measurement uncertainty

Numerical simulation was employed to determine the extent of heat loss from the test module. A 3D model of the test module was constructed in which electrical power input is simulated by a uniform heat flux along the inner walls of the cartridge heater bores. Direct estimation of heat loss is complicated by the boundary condition along the heated surface. Because the two-phase heat transfer coefficient cannot be directly measured, numerical iteration is required. An initial value of the heat transfer coefficient is determined by equating the rate of heat transferred to the water to the electrical power input (*i.e.*, by assuming zero heat loss), and using the measured mean surface and mean fluid temperatures. This value is then adjusted numerically until the predicted mean temperature at the thermocouple plane matches the measured mean temperature. The maximum heat loss is estimated at 6–10% of the electrical power input for single-phase and two-phase conditions, respectively. Therefore, all heat flux data presented in this study are set equal to the total electrical power input divided by the heated surface area of the copper block.

Additional measurements uncertainties are attributed to the instrumentation used in the study. The wattmeter used to measure the electrical power input has an accuracy of 0.5%. The uncertainties in the pressure and temperature measurements are estimated at 3.5% and ±0.3 °C respectively, and the flow rate measurement uncertainty is 4%.

2.5. Carbon nanotube surface preparation

CNT growth is achieved with the aid of a tri-layer metal catalyst [16] in combination with H_2 and CH_4 as feed gases in a microwave plasma chemical vapor deposition chamber (MPCVD). Different metal catalysts have been used in the past for carbon nanotube growth. In this study, a tri-layer metal catalyst consisting of titanium, aluminum and iron provided good growth on the copper wall. The titanium under-layer provides surface bonding sites for CNTs that are well anchored to the copper surface. The anchoring of CNTs to the surface is crucial for two reasons. First, good anchoring greatly reduces thermal contact resistance between the CNTs and the surface, leading to minimal resistance to heat transfer [15]. Second, well-anchored CNTs possess greater resistance to detachment by shear forces exerted by the fluid flow.

2.5.1. Tri-layer metal catalyst surface preparation

The first step of the CNT growth involves cleaning the top surface of the test module's copper block in water, acetone and methanol. The copper wall is then placed in a three-target Varian electron-beam metal evaporation chamber. In the authors' preliminary study [13], a 30-nm titanium layer was deposited first in the chamber, followed sequentially by 15 nm of aluminum and 9 nm of iron. For the present study, a similar tri-layer catalyst is used but with a thicker titanium base to avoid catalyst contamination from the copper block. A 60-nm titanium layer is deposited first, followed sequentially by 10 nm of aluminum and 3 nm of iron. The purpose of the aluminum layer is to promote the segregation of annealed iron nanoparticles [17].

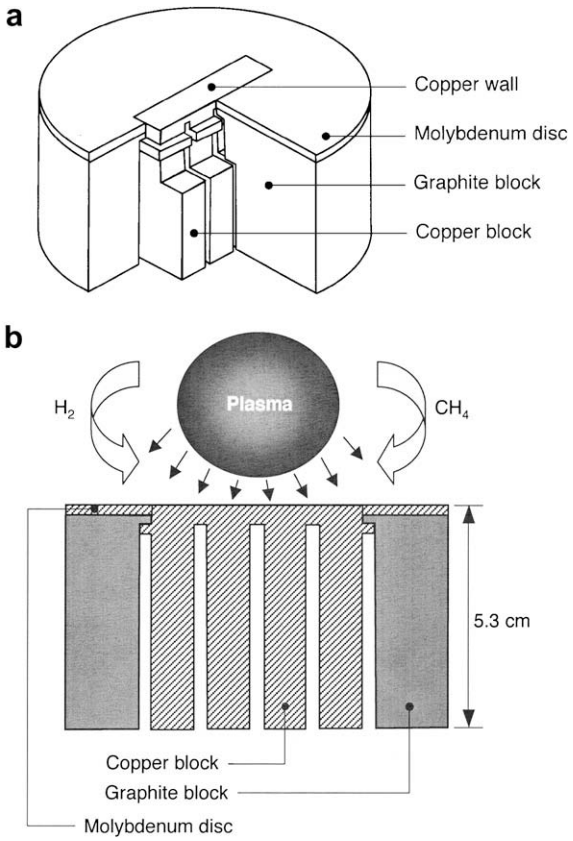

Fig. 3. (a) Schematic of graphite fixture. (b) Experimental setup for CNT growth in MPCVD reactor.

2.5.2. Microwave plasma chemical vapor deposition (MPCVD) system growth

A SEKI AX5200S MPCVD reactor [18] was used for the CNT growth. Because of the large size of the copper block, a graphite fixture was fabricated to shield the uncoated surfaces of the copper block from the microwave plasma, and also to prevent plasma concentration along the sharp metal edges. Shown in Fig. 3(a), the graphite fixture was machined from a solid cylinder that was hollowed out in the center to the outer dimensions of the copper block. All edges of the graphite fixture were carefully chamfered to prevent adverse plasma concentration. The copper surface penetrated a rectangular hole of the same size ($44.8 \times 10.0\ mm^2$) in the top surface of the graphite fixture. To concentrate the plasma directly above the test surface, a 3.175-mm thick chamfered molybdenum puck, also having a $44.8 \times 10.0\ mm^2$ central rectangular hole, was placed atop the graphite fixture to produce a surface that is flush with the copper surface. The assembly, with the tri-layer metal catalyst deposited onto the copper surface, was then placed on top of a graphite susceptor in the chamber. Fig. 3(b) shows a schematic of the experimental setup for CNT growth in the MPCVD reactor. The plasma was powered by a 1.5 kW (2.45 GHz) ASTex AX2100 microwave generator. Inductive substrate heating was supplied by a 3.5 kW radio-frequency coil and power supply beneath the susceptor.

The synthesis protocol used for CNT growth involved annealing, hydrogen plasma ignition, and introduction of carbon-containing gas species. Before supplying the feed gases (H_2 and CH_4), the test surface was annealed in N_2 at 50 sccm for 10 min using the induction heater. The N_2 feed was stopped when the temperature of the test surface reached approximately 700 °C as measured by a dual-wavelength Williamson pyrometer. Immediately thereafter, the chamber was evacuated, and then the H_2 was introduced at 50 sccm until the chamber pressure reached 10 torr. At this point, the plasma was ignited at 300 W, and then the CH_4 was introduced at 10 sccm. With the plasma above the copper wall, the pyrometer indicated a temperature of approximately 800 °C. The CNT synthesis process was terminated after 10 min to achieve sufficient CNT array height, and the reactor was evacuated. The sample was allowed to cool to room temperature before being removed from the chamber. Fig. 4(a) shows a top view photograph of the copper block following the CNT growth. Table 3 provides complete details of the CNT synthesis for the authors' preliminary study [13] and those of three different copper block surfaces that were tested in the present study.

The large size of the copper heat sink posed a problem when acquiring scanning electron microscopy (SEM) images of the CNT-coated surface. In order to better characterize the CNT growth, a small copper sample with the same surface finish and same tri-layer catalyst was placed next to the copper block in the MPCVD chamber. This sample provided a good representation of the quality and morphology of CNTs anchored to the heater surface of the copper block. All SEM images of the CNT-coated surface prior to testing that are presented in this study are those of small copper samples treated in the same manner as the corresponding copper block's heated surface.

2.6. Test surfaces

2.6.1. Bare copper surface

To understand the enhancement benefits of CNTs, thermal results with CNT-coated surfaces are compared to those with bare copper. The bare copper surface was vapor blasted to provide an abundance of surface cavities as large as 3 μm. Fig. 4(b) shows SEM images of the vapor blasted bare copper surface.

2.6.2. CNT-coated copper surface

In the authors' preliminary study [13], a single CNT-coated copper surface was used for all tests. For the present study, three identical copper blocks were fabricated that were coated with CNTs using the growth conditions described earlier. Fig. 4(b) shows SEM images for two of the surfaces tested in the present study. The resulting CNT array appears to be dense with MWCNTs approximately 60 nm in diameter.

3. Flow visualization results

A flow visualization technique was employed using a high-speed video imaging system to capture two-phase flow patterns and interfacial phenomena in the micro-channel. Optical access to the micro-channel was provided by the transparent test module's cover plate in a direction normal to the flow. A Photron FASTCAM-Ultima APX FM camera, interfaced to a computer, was utilized to record both video sequences and still images of the flow. In the authors' preliminary study [13], similar flow visualization techniques provided valuable insight into differences in flow boiling behavior between CNT-coated and bare copper surfaces.

The flow visualization study discussed in this paper is focused on capturing key aspects of the flow such as the onset of boiling, two-phase flow behavior and CHF for three mass velocities (G = 86, 228 and 368 kg/m^2 s) at T_{in} = 30 °C over a period of time. Temporal changes of the flow behavior are vital to understanding any time-dependent degradation of the heat transfer performance.

3.1. Onset of nucleate boiling

For the relatively low mass velocity case corresponding to G = 86 kg/m^2 s, bubbles began to nucleate on the CNT-coated surface in the downstream region of the micro-channel. Due to the large width of the micro-channel, the nucleating bubbles quickly coalesced

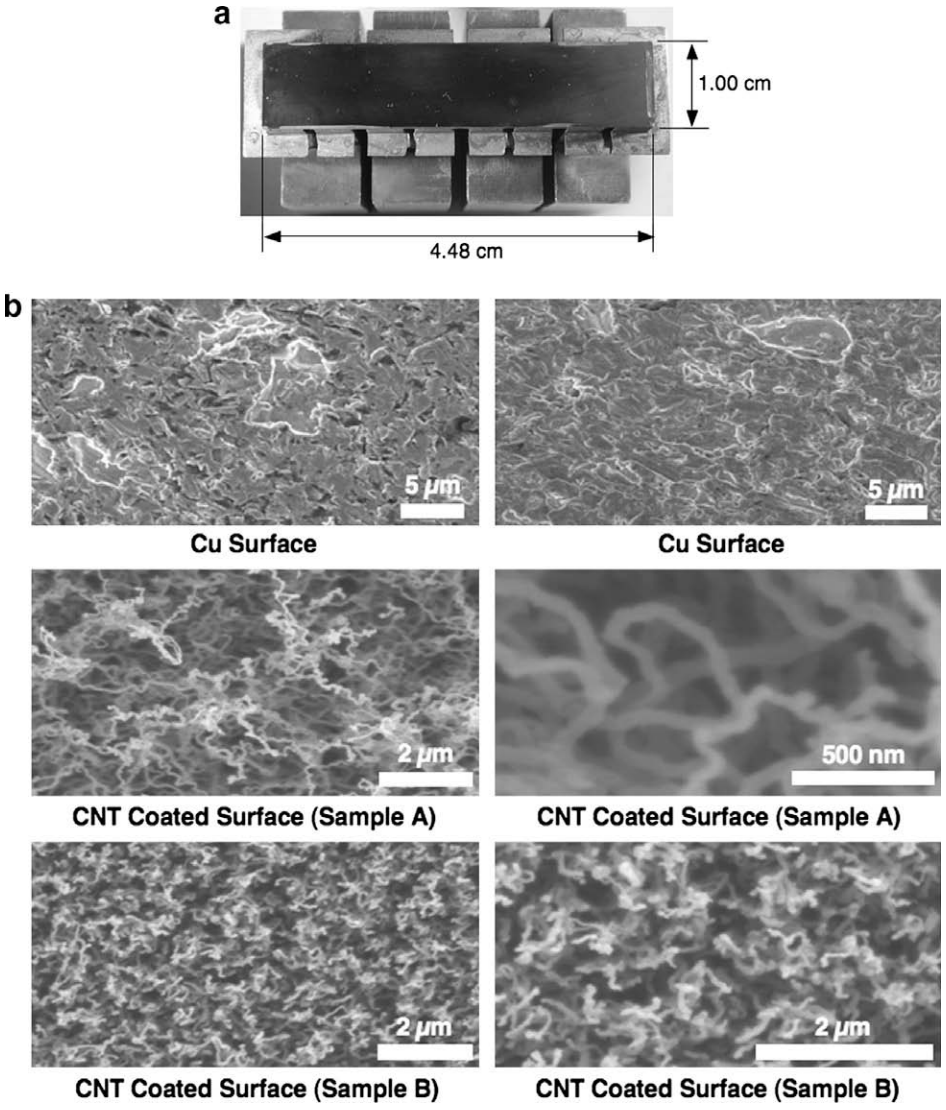

Fig. 4. (a) Photograph of copper block showing top surface coated with CNTs. (b) SEM images of different test surfaces.

Table 3
Synthesis parameters for CNT surfaces.

	Preliminary study sample	Present study		
		Sample A	Sample B	Sample C
Ti/Al/Fe thickness [nm]	30/15/9	60/10/3	60/10/3	60/10/3
Pyrometer temperature before plasma strike [°C]	650	645	634	758
CH_4 flow rate [sccm]	10	10	10	10
H_2 flow rate [sccm]	50	50	50	50
Microwave power [W]	300	300	300	300
Growth time [min]	10	10	10	10

Sample A, B and C are used for low, mid and high mass velocity tests, respectively.
Pyrometer temperature is the temperature of the top surface of the copper block before the plasma is switched on. This is the temperature of the surface after 10 min of annealing the surface in N_2.

into a single slug-type bubble as shown in Fig. 5(a). This behavior persisted at slightly higher heat flux levels, albeit with differences in shape, size and location of the slug bubble. Notice that the three images in Fig. 5(a) correspond to different repeatability tests.

For the higher mass velocity case of $G = 368$ kg/m^2 s, boiling behavior was highly dependent on test sequence. As shown in Fig. 6(a), the onset of boiling for test 1 was associated with significant bubble formation downstream. Subsequent tests (2 and 3) witnessed an appreciable monotonic reduction in the number of nucleation sites and boiling vigor. Furthermore, boiling commenced at lower heat fluxes for tests 2 and 3 compared to test 1, suggesting substantial physical changes to the CNT-coated surface at this high mass velocity.

3.2. Two-Phase flow pattern development

For $G = 86$ kg/m^2 s, mostly of slug-type bubbles were observed throughout the repeatability tests as shown in Fig. 5(b). For

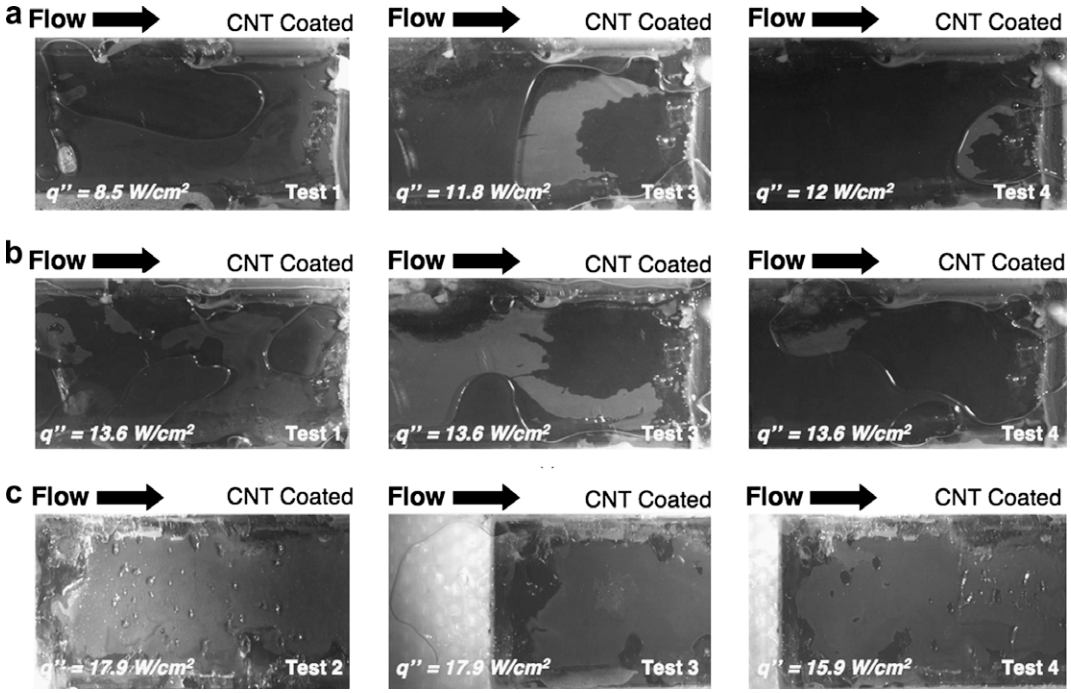

Fig. 5. Images of boiling behavior in micro-channel with CNT-coated surface at $G = 86$ kg/m^2 s for (a) onset of boiling in downstream region, (b) two-phase flow pattern in downstream region, and (c) vapor backflow at CHF in upstream region.

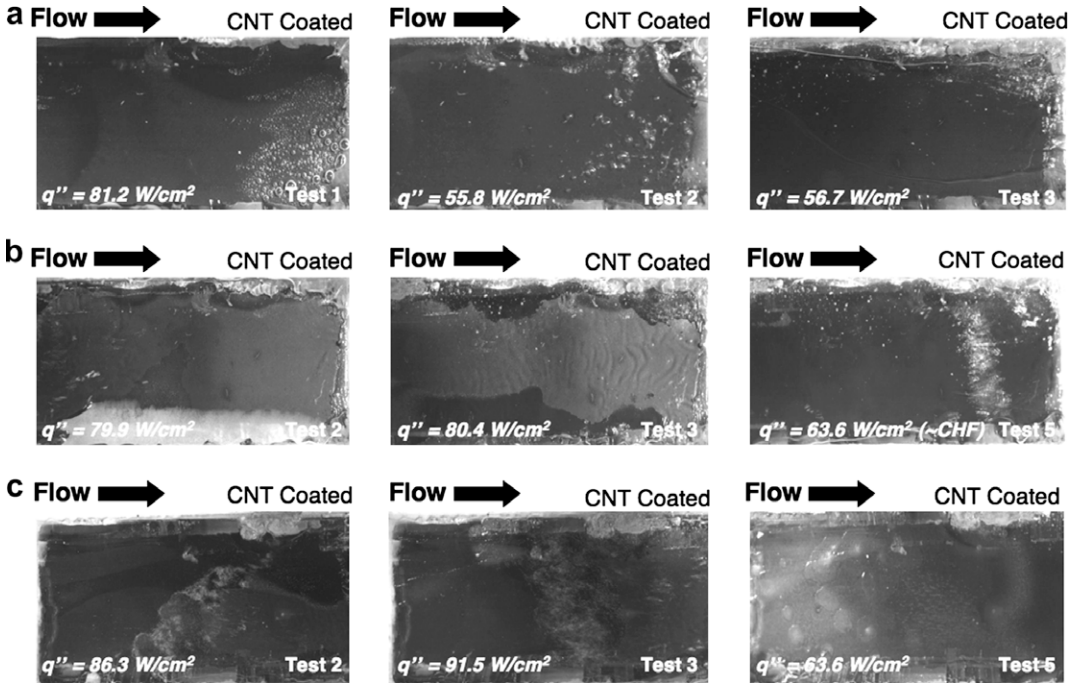

Fig. 6. Images of boiling behavior in micro-channel with CNT-coated surface at $G = 368$ kg/m^2 s for (a) onset of boiling in downstream region, (b) two-phase flow pattern in downstream region, and (c) vapor backflow at CHF in upstream region.

$G = 368$ kg/m^2 s, annular flow was dominant for all repeatability tests as shown in Fig. 6(b). However, the transition to annular flow for test 5 occurred at a much lower heat flux than for tests 2 or 3. This further points to appreciable physical changes to the CNT-coated surface following repeated tests at high mass velocity.

3.3. Critical heat flux

CHF in the micro-channel was triggered by vapor backflow in a manner similar to that reported in the authors' preliminary study [13]. Fig. 5(c) shows the vapor back flow in the upstream region of the micro-channel for three of the repeatability tests at $G = 86$ kg/m^2 s. It is important to note that vapor flow reversal near CHF is intrinsic to many types of micro-channel flows, not only those with CNT-coated surfaces. This reversal results from a significant increase in pressure drop at high heat fluxes as a large fraction of the liquid flow is converted to vapor [4,19,20]. This increases upstream pressure, momentarily forcing vapor backward into the inlet and preventing liquid from entering the micro-channel. Pressure in the upstream plenum continues to rise until it is able to

overcome the high pressure drop across the micro-channel itself. This enables the liquid to re-enter the micro-channel and purge the accumulated vapor. Thereafter, the boiling process is repeated and vapor accumulates and reverses flow direction until liquid is able once again to enter the micro-channel. This process is associated with appreciable oscillations in pressure, flow rate, and surface temperature, and these oscillations amplify with each vapor purge cycle until the surface temperature begins to escalate uncontrollably, signaling the commencement of CHF. A more detailed discussion on this important topic is provided in the next section.

This vapor flow reversal mechanism was a precursor to CHF in all repeatability tests, which occurred at about the same heat flux for all tests at the low mass velocity as shown in Fig. 5(c). However, this CHF phenomenon occurred at drastically different heat fluxes at the high mass flux of $G = 368$ kg/m^2 s. Fig. 6(c) shows that CHF occurred at $q'' = 63.6$ W/cm^2 for test 5 in comparison to $q'' = 86.3$ W/cm^2 for test 2. Here again, the profound degradation in boiling performance points to appreciable physical changes to the CNT-coated surface at the highest mass velocity. These changes will become more apparent from SEM images presented later in this study.

4. Experimental results and discussion

4.1. Pressure drop characteristics and two-phase instabilities

A temporal study of single-phase pressure drop is used to explore pressure drop trends for the bare copper surface and the three CNT-coated surfaces. Fig. 7(a) reveals that pressure drop for the bare surface remains constant over time but increases with increasing mass velocity. Notice that for each mass velocity, pressure drop is higher for the CNT-coated surface compared to the bare copper surface and the difference increases with increasing mass velocity. This difference can be explained by the increased shear stress with the CNT-coated surfaces, which is brought about by increased surface roughness and turbulence. Results for the CNT-coated surfaces indicated that pressure drop at $G = 86$ and 228 kg/m^2 s is fairly constant over time. However, at $G = 368$ kg/m^2 s, the pressure drop increases monotonically over time, which further points to significant physical changes to the CNT-coated surface at the highest mass velocity.

Two-phase instabilities have been a major topic of research for many decades. Hydrodynamic instabilities exist in a wide variety of two-phase systems and understanding their mechanism is crucial from a design standpoint. Qu and Mudawar [21] identified two types of hydrodynamic instability that occur in micro-channel heat sinks. The first is *severe pressure drop oscillation*, which is associated with interaction between the vapor generation in the heat sink and the compressible volume in the flow loop upstream of the heat sink. They demonstrated that this form of instability may be virtually eliminated by throttling the flow with the aid of a control valve situated upstream of the heat sink. The second type of instability is a relatively *mild flow instability* caused by two-phase flow interactions intrinsic to the heat sink itself; this type of instability cannot be eliminated with upstream throttling. Qu and Mudawar [4] showed that even this milder form of instability begins to amplify significantly as CHF is approached as discussed earlier. In fact, CHF occurs when the instability becomes strong enough to push vapor backwards into the inlet plenum, blocking the flow of incoming liquid. A more detailed discussion of the temporal aspects of this instability at CHF is provided in [19–21].

While the present micro-channel module features a hydraulic diameter equal to that employed by Qu and Mudawar in their parallel micro-channel module, the present micro-channel eliminated any instabilities associated with interaction between micro-channels. Thus, any instabilities must be associated with two-phase mixture interactions spanning the 10-mm width of the micro-channel. In any case, instabilities also intensified in the present micro-channel as well as CHF approached. Fig. 7(b) shows temporal records of

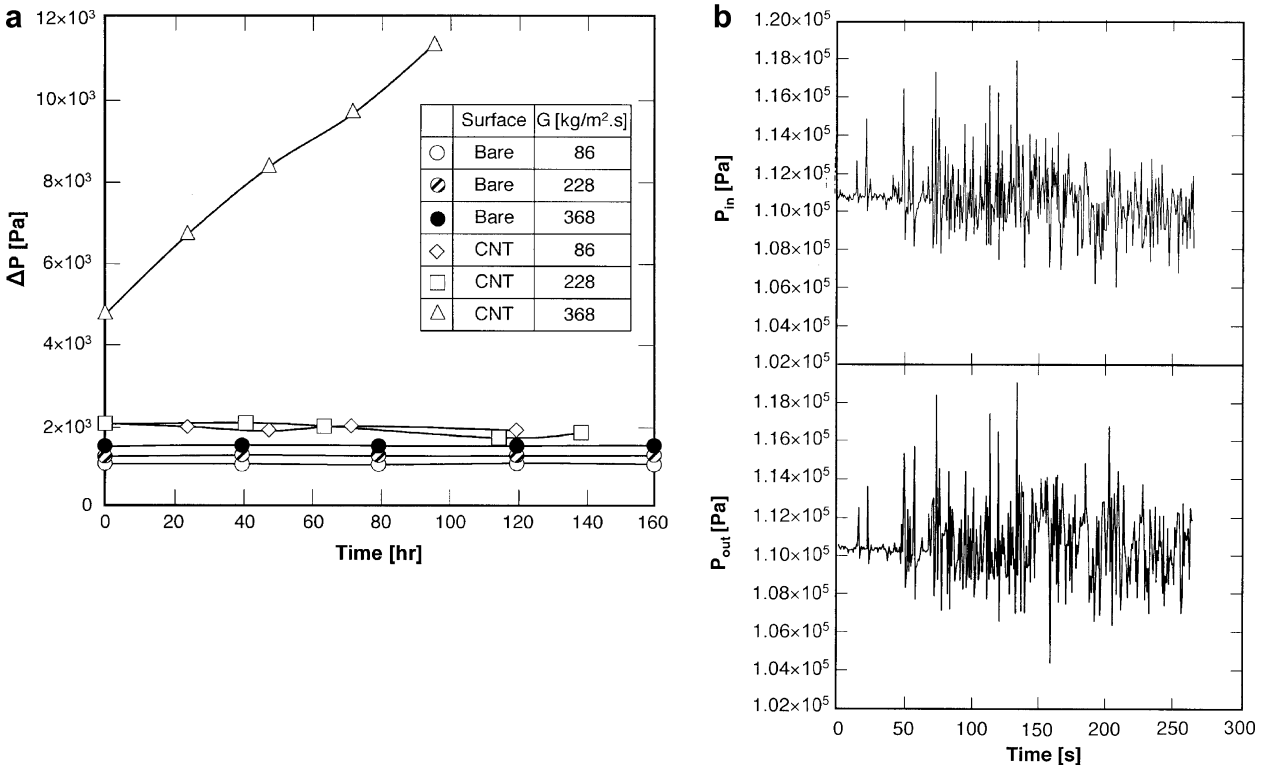

Fig. 7. (a) Variation of single-phase pressure drop with time for bare and CNT-coated surfaces at different mass velocities and $T_{in} = 30$ °C. (b) Temporal records of inlet plenum pressure and outlet plenum pressure for flow boiling on bare surface at $G = 299$ kg/m^2 s, $T_{in} = 30$ °C and $q'' = 46.9$ W/cm^2.

the measured inlet and outlet plenum pressures measured at $G = 299$ kg/m^2 s and $T_{in} = 30$ °C for a heat flux of $q'' = 46.9$ W/cm^2, which is close to CHF. Like the studies by Qu and Mudawar [4,21] and Lee and Mudawar [19,20], CHF was associated with vapor backflow towards the inlet plenum, which triggered large temperature fluctuations in the copper block. In some situations, the intensified instability was manifest by large vertical oscillations of the rotameter's float.

4.2. Boiling curve and CHF results

The need to utilize different CNT-coated surfaces for different series of tests and to explore any CHF variations with time is readily apparent from the authors' previous CHF data [13]. Fig. 8(a) shows the variation of CHF with mass velocity for both the bare and CNT-coated surfaces for two inlet subcooling levels. For the lowest mass velocity of 86 kg/m^2 s, the CNT-coated surface enhanced CHF by 23% at $T_{in} = 30$ °C and 21% at $T_{in} = 60$ °C. The enhancement diminished for the intermediate mass velocity of $G = 228$ kg/m^2 s to 3% for $T_{in} = 30$ °C and 21% for $T_{in} = 60$ °C. The CHF performance of the CNT-coated surface was further compromised at the highest mass velocity of $G = 368$ kg/m^2 s, yielding a 22% reduction in CHF for $T_{in} = 30$ °C and only 3% enhancement for $T_{in} = 60$ °C.

In order to acquire a more complete CHF database, more data points were collected by performing additional tests with the same bare and CNT-coated surfaces at intermediate mass velocities within the range of 86–368 kg/m^2 s. Fig. 8(b) shows that the bare surface follows the expected trend of CHF increasing monotonically with increasing mass velocity. However, the new data for the CNT-coated surface produced an unexpected reduction in CHF values from the trend captured by the initial data. This points to appreciable time-dependent morphological changes to the CNT-coated surface.

This important finding prompted the authors to adopt a new, more systematic data taking scheme, where tests with the same CNT-coated surface and same inlet temperature and mass velocity are repeated over a 24 h period in order to ascertain the time dependence of CHF. Three different CNT-coated surfaces were fabricated for this purpose; one was used with each of three mass velocities.

Fig. 9 shows, for the CNT-coated surface, subcooled flow boiling curves obtained from temperature measurements at the four thermocouple locations (z_{tc1} to z_{tc4}) for three mass velocities ($G = 86$, 228, 368 kg/m^2 s) and an inlet temperature of $T_{in} = 30$ °C. The boiling curves are based on the difference between surface temperature at a particular thermocouple location, $T_{w,tci}$, and T_{in}, where $T_{w,tci}$ is determined from the assumption of one-dimensional heat conduction between the corresponding thermocouple and the heated surface $T_{w,tci} = T_{tci} - q''H_{th}/k_s$. For all four thermocouple locations, the boiling curves possess constant slope at low heat fluxes corresponding to the single-phase region. An increase in slope marks the onset of boiling, which is first detected at the surface above the thermocouple farthest from the inlet (z_{tc4}), where fluid temperature is highest, and then propagates upstream with increasing heat flux. For the highest mass velocity of $G = 368$ kg/m^2 s, surface temperature variations are appreciably larger than those for $G = 86$ and 228 kg/m^2 s. CHF is first detected by the most downstream thermocouple (*tc4*) in the form of a rapid unsteady temperature rise. This rise quickly propagates upstream towards the inlet.

Fig. 10 shows for, each of three mass velocities, subcooled boiling curves for three sequential tests with the same CNT-coated surface compared to data for the bare copper surface. For the lowest mass velocity of $G = 86$ kg/m^2 s, Fig. 10(a) reveals that the boiling curves for the CNT-coated surface shifted toward higher surface temperatures, *i.e.*, poorer heat transfer performance compared to the bare surface. Furthermore, CHF values for all three CNT-coated surface tests are smaller than for the bare copper surface. All three tests feature similar shape and magnitude of both single-phase and two-phase heat transfer coefficients, as well as about equal CHF values.

For $G = 228$ kg/m^2 s, Fig. 10(b) shows that tests 1 and 2 with the CNT-coated surface provide slight enhancement in both the single-phase and nucleate boiling regions, and substantial enhancement in CHF. However, this enhancement is completely lost with test 3. Furthermore, there is a substantial decrease in CHF compared to tests 1 and 2.

For the highest mass velocity of $G = 368$ kg/m^2 s, Fig. 10(c) shows significant enhancement in the single-phase heat transfer coefficient with the CNT-coated surface compared to the bare copper surface. The three CNT-coated surface tests show fairly similar

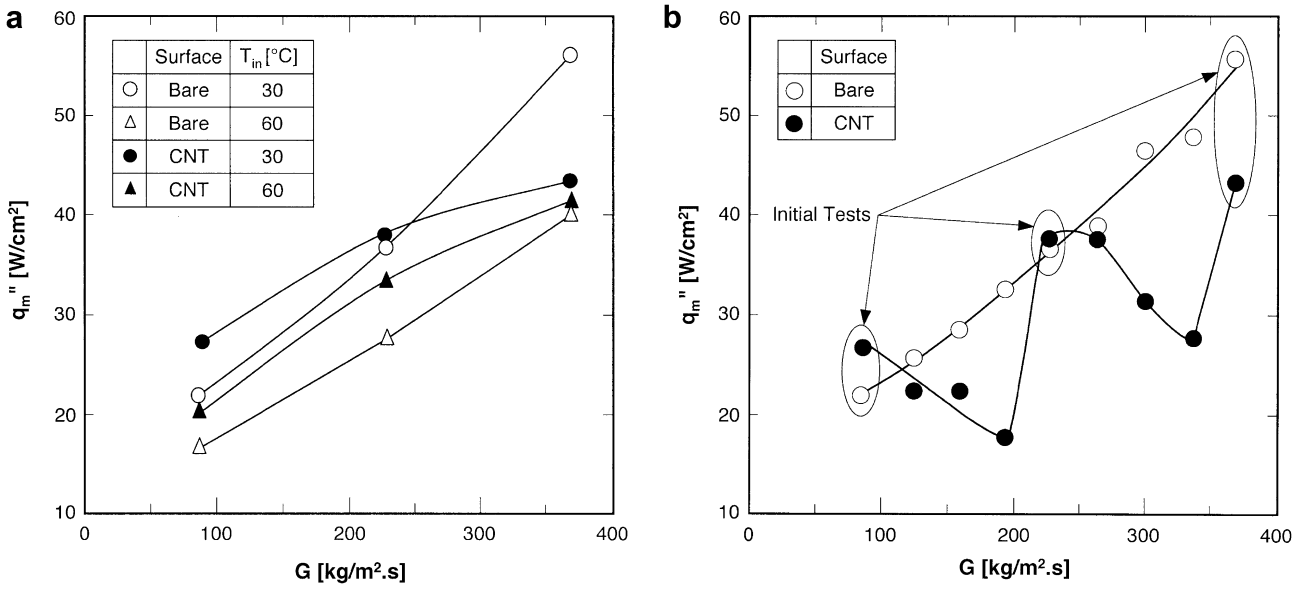

Fig. 8. Variation of CHF with mass velocity measured during preliminary tests for bare and CNT-coated surfaces for (a) $G = 86$, 228 and 368 kg/m^2 s at $T_{in} = 30$ and 60 °C and (b) $G = 86$–368 kg/m^2 s at $T_{in} = 30$ °C.

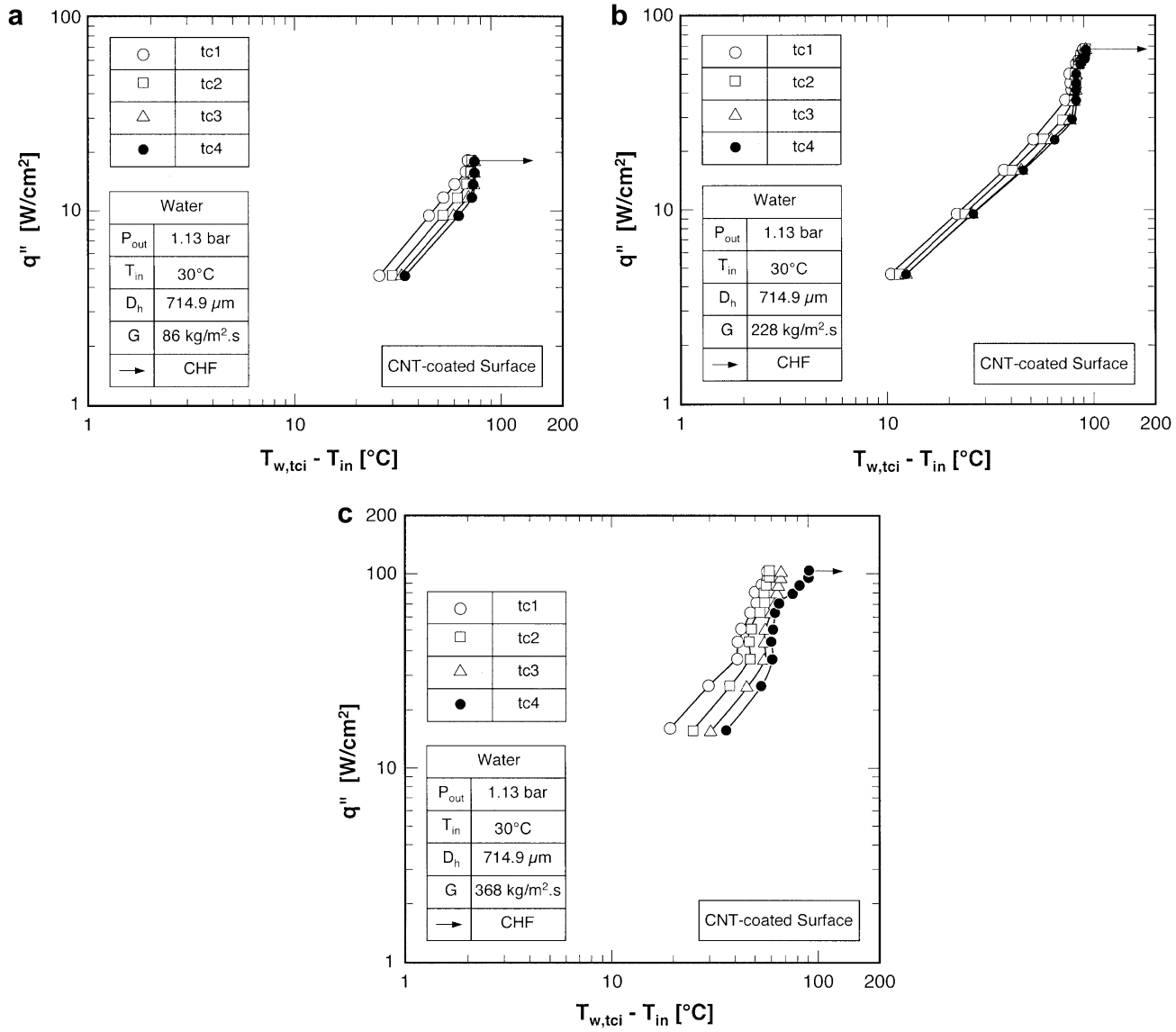

Fig. 9. Subcooled flow boiling curves measured at four heater block thermocouples at T_{in} = 30 °C during the first test in repeatability sequence with (a) CNT-coated surface for G = 86 kg/m^2 s, (b) CNT-coated surface for G = 288 kg/m^2 s, and (c) CNT-coated surface for G = 368 kg/m^2 s.

single-phase results, but the trends are quite different in the nucleate boiling region. Test 1 shows the most superior two-phase performance, indicating some surface degradation with the two subsequent tests. Also, while CHF values for all three CNT-coated surface tests are higher than for the bare copper surface, there is appreciable degradation in CHF for the CNT-coated surface following test 1.

The temporal study of boiling performance for the three mass velocities reveals important trends that help explain the causes of CNT-surface degradation. Fig. 11 shows temporal records of CHF for the CNT-coated surfaces corresponding to the three mass velocities. The time coordinate indicates the moment that CHF was detected in a given test. For the lowest mass velocity of G = 86 kg/m^2 s, CHF is fairly constant after five consecutive tests. This suggests that the corresponding fluid velocity is too small to influence the CNT coating. For G = 228 kg/m^2 s, the CHF degradation is significant after the second test. For the highest mass velocity of G = 368 kg/m^2 s, CHF degradation is severe and is observed starting with test 2 (first repeatability test). This proves high flow velocities have a significant influence on the CNT coating. Table 4 provides CHF values measured during the three consecutive tests with each of the three CNT-coated surfaces.

Performance differences between the CNT-coated surfaces tested in the present study and those used in the authors' prior study [13] can be attributed to different CNT growth protocols. These differences, which can influence CNT quality, height and anchoring to the copper surface, can be attributed to the different tri-layer catalyst thicknesses used in the CNT growth. A 60-nm titanium base was deposited in the present study compared to 30 nm in the earlier study. This increase served to resist catalyst poisoning from the copper surface, which caused CNT growth to fail occasionally in the earlier study. In addition, a 3-nm Fe layer was deposited in the present study compared to 9 nm in the earlier study. With these thickness changes, catalyst contamination was fully eliminated and all CNT growths were successful.

4.3. Morphology of CNT-coated surface after flow boiling

As described by Chakrapani et al. [11], capillary forces during surface fluid evaporation from a horizontal CNT-coated surface

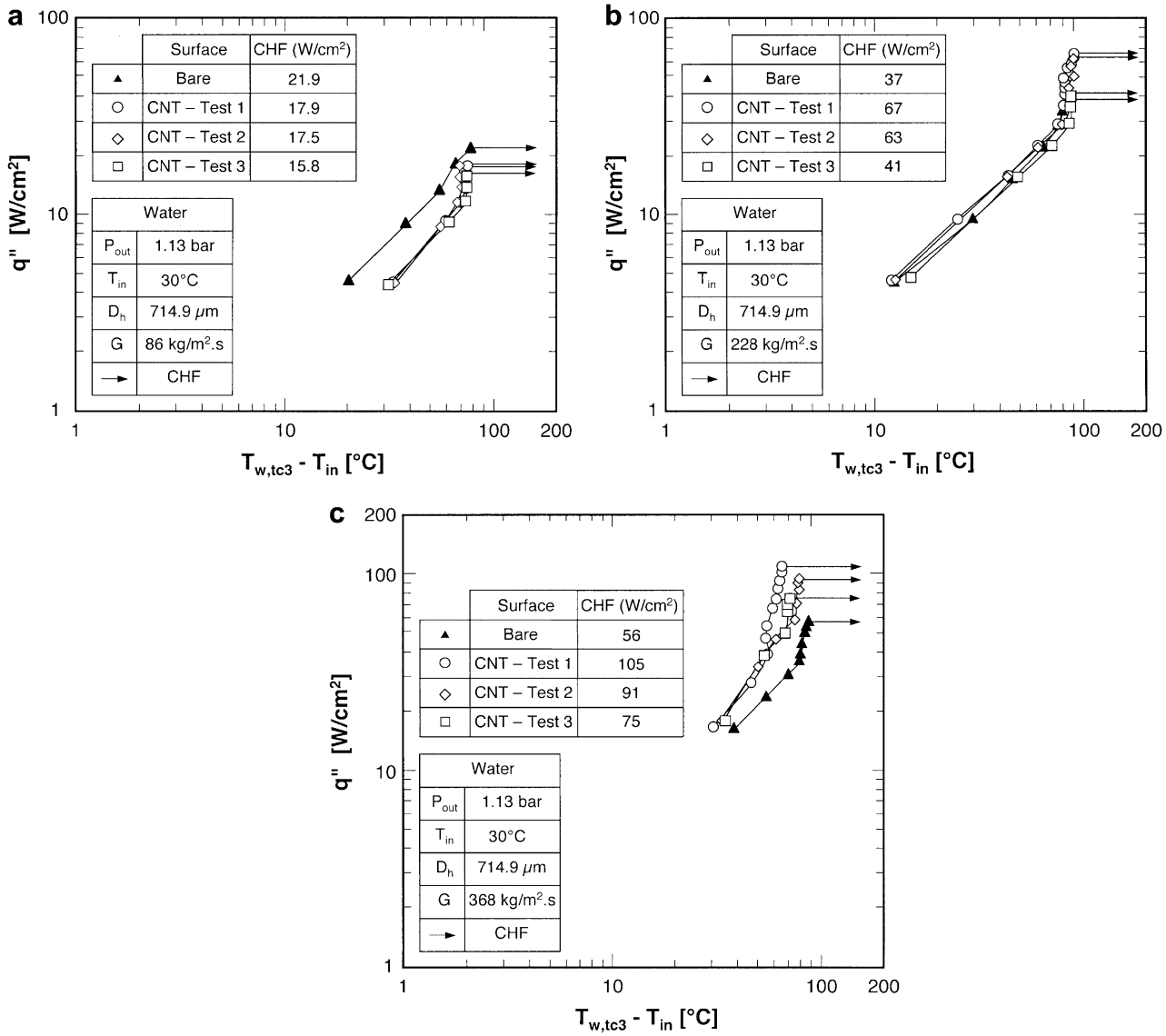

Fig. 10. Subcooled flow boiling curves measured at z_{tc3} for T_{in} = 30 °C and (a) G = 86 kg/m^2 s, (b) G = 228 kg/m^2 s, and (c) G = 368 kg/m^2 s.

cause initially vertical CNTs to regroup into an array of cells whose walls consist of vertical CNTs that are bunched together, surrounding central depressions consisting of CNTs that are bent and collapsed upon the substrate surface. This phenomenon was attributed to the high degree of flexibility of CNTs.

The bending behavior is evident from SEM images of the CNT-coating following boiling tests in the present study as well. Because the copper block was too large to obtain SEM images of the CNT-coated surface after the boiling tests, a thin layer (~1 mm) of the top surface of the copper block was sliced off and used for image collection. Unlike the study by Chakrapani et al., where bending relied on relatively weak capillary forces, the morphological changes in the present study are far more severe because of the combined effects of bubble nucleation and fluid flow. Fig. 12 shows the extent of morphological changes in the present study following a series of five tests at T_{in} = 30 °C and the highest mass velocity of G = 368 kg/m^2 s. Shown in Fig. 12(a) are cellular CNT formation virtually identical to those described by Chakrapani et al. [11]. These cells were observed on isolated regions of the surface. The middle image in Fig. 12(a) shows a cavity formed within the raised outer wall of adjacent cells. The right-hand image in Fig. 12(a) shows a thick formation caused by bunching of a large number of CNTs; there is no evidence of CNT loss due the shear forces exerted by the liquid flow. However, the most dominant CNT pattern that was captured on the boiling surface was the dramatic '*fish scale*' formations caused by bending and bunching of CNTs into fairly ordered triangular shapes as illustrated in Fig. 12(b). The '*fish scale*' structures appear to overlap and form voids in between.

4.4. Overall assessment of CNT enhancement and degradation trends

The profound changes to the morphology of the CNT-coated surface depicted in Fig. 12 help explain the many complex heat transfer enhancement and degradation trends presented earlier in this study. The SEM images demonstrate that high velocities cause appreciable bending or folding of CNTs upon the heated wall. Furthermore, the *'fish scales'* overlap to create flat voids. This pattern has three important influences on heat transfer performance consequences. First, the voids provide near-zero-angle cavities that are ideal for bubble nucleation. This is quite apparent in Fig. 10(c) in the form of appreciable heat transfer enhancement in the nucleate boiling region for all three tests at G = 368 kg/m^2 s as compared

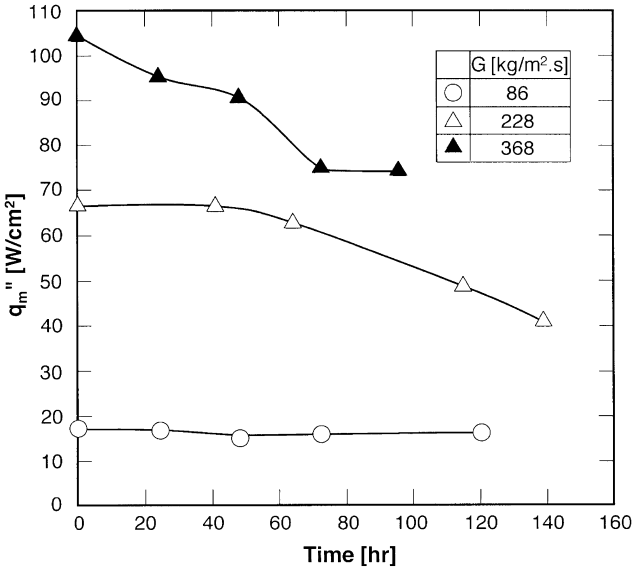

Fig. 11. Variation of CHF with time for CNT-coated surfaces for three mass velocities and T_{in} = 30 °C.

Table 4
CHF data from five test runs with each of the CNT-coated surfaces.

	q''_m[W/cm^2]		
	G = 86 [kg/m^2 s] (Sample A)	G = 228 [kg/m^2 s] (Sample B)	G = 368 [kg/m^2 s] (Sample C)
Test 1	17.9	67	105
Test 2	17.5	66.5	96
Test 3	15.8	63	91.5
Test 4	16.3	49.1	75.9
Test 5	16.7	41.3	75

to the bare copper surface. Second, CHF is enhanced with the CNT coating at G = 228 and 368 kg/m^2 s due to the increased heat transfer area associated with the *'fish scales.'* Third, the CHF enhancement for the same two mass velocities decreases with time as the initially vertical CNTs are gradually folded upon the heated surface. Since CNTs and CNT scales can act as very high conductivity fins that penetrate into the cooler, bulk liquid to take advantage of the bulk subcooling away from the wall, CNT folding greatly compromises CHF enhancement over time.

5. Conclusions

This study examined the heat transfer enhancement benefits of coating the bottom wall of a shallow rectangular micro-channel with CNTs. Lessons learned from a previous study by the authors [13] were the premise for a new testing protocol to ensure systematic assessment of the repeatability of heat transfer results. Using water as the working fluid, experiments were performed with a bare copper surface and three different, yet identical CNT-coated surfaces. Each of the CNT-coated surfaces was tested repeatedly at the same mass velocity to explore any time dependence of heat transfer performance parameters, especially CHF. The study was supported by flow visualization using high-speed video imaging. Key findings from the study are as follows.

(1) The bare and CNT-coated surfaces share several similarities in boiling behavior. Boiling is always initiated in the downstream region of the micro-channel. Fluctuations in both inlet and outlet pressure intensify with increasing heat flux, especially near CHF. CHF is triggered by vapor backflow into the upstream plenum, which results in dryout over much of the heated surface.
(2) There are appreciable differences in the influence of CNT coating on boiling performance at high mass velocities as compared to low. The CNT coating increases pressure drop, especially at high mass velocities. CHF results are quite repeatable for the bare surface at all mass velocities and the CNT-coated surface at only the low mass velocity of G = 86 kg/m^2 s. However, CHF is degraded following repeated tests at the higher mass velocities of G = 228 and 368 kg/m^2 s. This degradation proves high flow velocities cause appreciable changes to the morphology of the CNT-coated surface.
(3) SEM images also reveal significant changes to the morphology of the CNT-coated surface following repeated tests at the high mass velocity of G = 368 kg/m^2 s. Initially near-vertical CNTs are bent upon the heated surface to form a repeated '*fish-scale*' pattern. This pattern is believed to influence heat transfer performance at high mass velocities in three different ways. First, voids between the *'fish scales'* provide

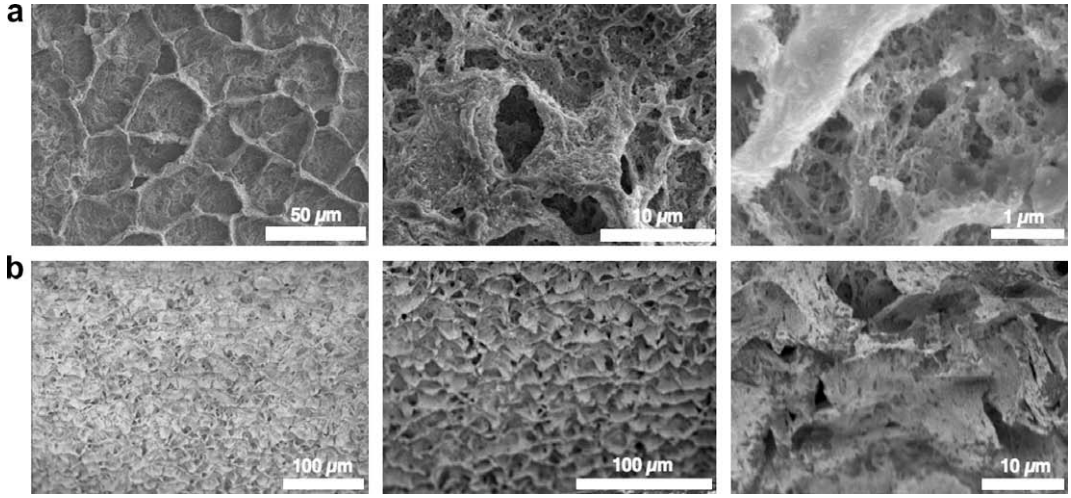

Fig. 12. SEM images of CNT-coated surface after five boiling tests at the highest mass velocity of G = 368 kg/m^2 s and T_{in} = 30 °C. (a) CNT cellular formations observed over isolated regions of the surface. (b) Dominant 'fish-scale' pattern observed over most of the surface.

near-zero-angle cavities that enhance heat transfer in the nucleate boiling region compared to the bare copper surface. Second, CHF is enhanced because of the increased heat transfer area associated with the *'fish scales.'* Third, the CHF enhancement decreases following repeated tests as the CNT fin effect is compromised by the continued CNT bending.

References

[1] I. Mudawar, Assessment of high-heat-flux thermal management schemes, IEEE Trans. Compon. Packag. Tech. 24 (2001) 122–141.
[2] I. Mudawar, D.E. Maddox, Critical heat flux in subcooled flow boiling of fluorocarbon liquid on a simulated electronic chip in a vertical rectangular channel, Int. J. Heat Mass Transfer 32 (1989) 379–394.
[3] T.C. Willingham, I. Mudawar, Forced convection boiling and critical heat flux from a linear array of discrete heat sources, Int. J. Heat Mass Transfer 35 (1992) 2879–2890.
[4] W. Qu, I. Mudawar, Measurement and correlation of critical heat flux in two-phase micro-channel heat sinks, Int. J. Heat Mass Transfer 47 (2004) 2045–2059.
[5] W. Qu, I. Mudawar, Transport phenomena in two-phase micro-channel heat sinks, ASME J. Electron. Packag. 126 (2004) 213–224.
[6] W. Qu, I. Mudawar, Flow boiling heat transfer in two-phase micro-channel heat sinks- I. Experimental investigation and assessment of correlation methods, Int. J. Heat Mass Transfer 46 (2003) 2755–2771.
[7] P. Kim, L. Shi, A. Majumdar, P.L. McEuen, Thermal transport measurements of individual multiwalled nanotubes, Phys. Rev. Lett. 87 (2001) 1–4.
[8] S. Ujereh, T. Fisher, I. Mudawar, Effects of carbon nanotube arrays on nucleate pool boiling, Int. J. Heat Mass Transfer 50 (2007) 4023–4038.
[9] S. Launay, A.G. Fedorov, Y. Joshi, A. Cao, P.M. Ajayan, Hybrid micro-nano structured thermal interfaces for pool boiling heat transfer enhancement, Microelectron. J. 37 (2006) 1158–1164.
[10] E. Dujardin, T.W. Ebbesen, H. Hiura, K. Tanigaki, Capillarity and wetting of carbon nanotubes, Science 265 (1994) 1850–1852.
[11] N. Chakrapani, B. Wei, A. Caarrillo, P.M. Ajayan, R.S. Kane, Capillarity-driven assembly of two-dimensional cellular carbon nanotube foams, Proc. Natl. Acad. Sci. 101 (2004) 4009–4012.
[12] M. R Falvo, G.J. Clary, Bending and buckling of carbon nanotubes under large strain, Nature 389 (1997) 582–584.
[13] V. Khanikar, I. Mudawar, T.S. Fisher, Flow boiling in a micro-channel coated with carbon nanotubes, in: Proc. ITherm 2008, Orlando, Florida, May 28–31, 2008, pp. 960–969.
[14] S.T. Huxtable, D.G. Cahill, S. Shenogin, L. Xue, R. Ozisik, P. Barone, M. Usrey, M.S. Strano, G. Siddons, M. Shim, P. Keblinski, Interfacial heat flux in carbon nanotube suspensions, Nat. Mater. 2 (2003) 731–734.
[15] B.A. Cola, J. Xu, C. Cheng, H. Hu, X. Xu, T.S. Fisher, Photoacoustic characterization of carbon nanotube array thermal interfaces, J. Appl. Phys. 101 (2007) 9. 054313.
[16] J. Xu, T.S. Fisher, Enhancement of thermal interface materials with carbon nanotube arrays, Int. J. Heat Mass Transfer 49 (2006) 1658–1666.
[17] M. Meyyappan, L. Delzeit, A. Cassell, D. Hash, Carbon nanotube growth by PECVD: a review, Plasma Sources Sci. Technol. 12 (2003) 205–216.
[18] M.R. Maschmann, P.B. Amama, A. Goyal, Z. Iqbal, R. Gat, T.S. Fisher, Parametric study of synthesis conditions in plasma-enhanced CVD of high-quality single-walled carbon nanotubes, Carbon 44 (2006) 10–18.
[19] J. Lee, I. Mudawar, Two-phase flow in high-heat-flux micro-channel heat sink for refrigeration cooling applications: Part 1 – Pressure drop characteristics, Int. J. Heat Mass Transfer 48 (2005) 928–940.
[20] J. Lee, I. Mudawar, Fluid flow and heat transfer characteristics of low temperature two-phase micro-channel heat sinks – Part 1: Experimental methods and flow visualization results, Int. J. Heat Mass Transfer 51 (2008) 4315–4326.
[21] W. Qu, I. Mudawar, Measurement and prediction of pressure drop in two-phase micro-channel heat sinks, Int. J. Heat Mass Transfer 46 (2003) 2737–2753.